# Direct current energy generators from conducting polymer-inorganic oxide junction

Hao Shao,‡ Jian Fang,‡ Hongxia Wang, Hua Zhou, Tong Lin*

Institute for Frontier Materials, Deakin University, Geelong, VIC 3216, Australia

‡First Authors with equal contribution to this work

*E-mail: tong.lin@deakin.edu.au

# Electronic Supplementary Information

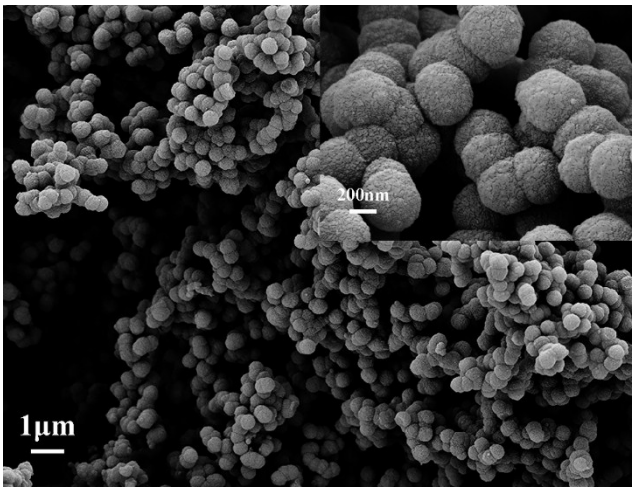


**Figure S1** SEM image of as-prepared PPy powders; Insert: high magnification of PPy powders.

Figure S1 shows a typical SEM image of the as-prepared PPy powders, their rough surface and a uniform size with average diameter of 500 nm can be observed from the high magnification SEM image (insert of Figure S1).

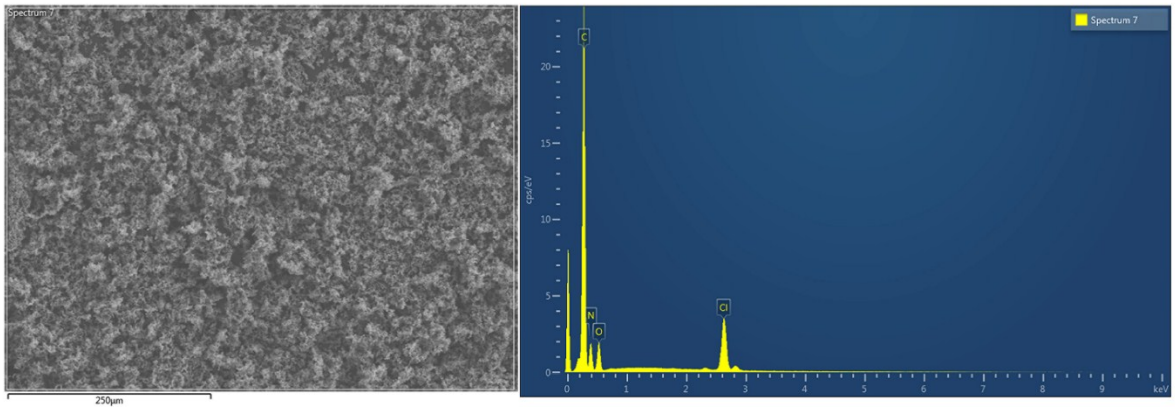


**Figure S2** EDX spectrum of as-prepared PPy powders.

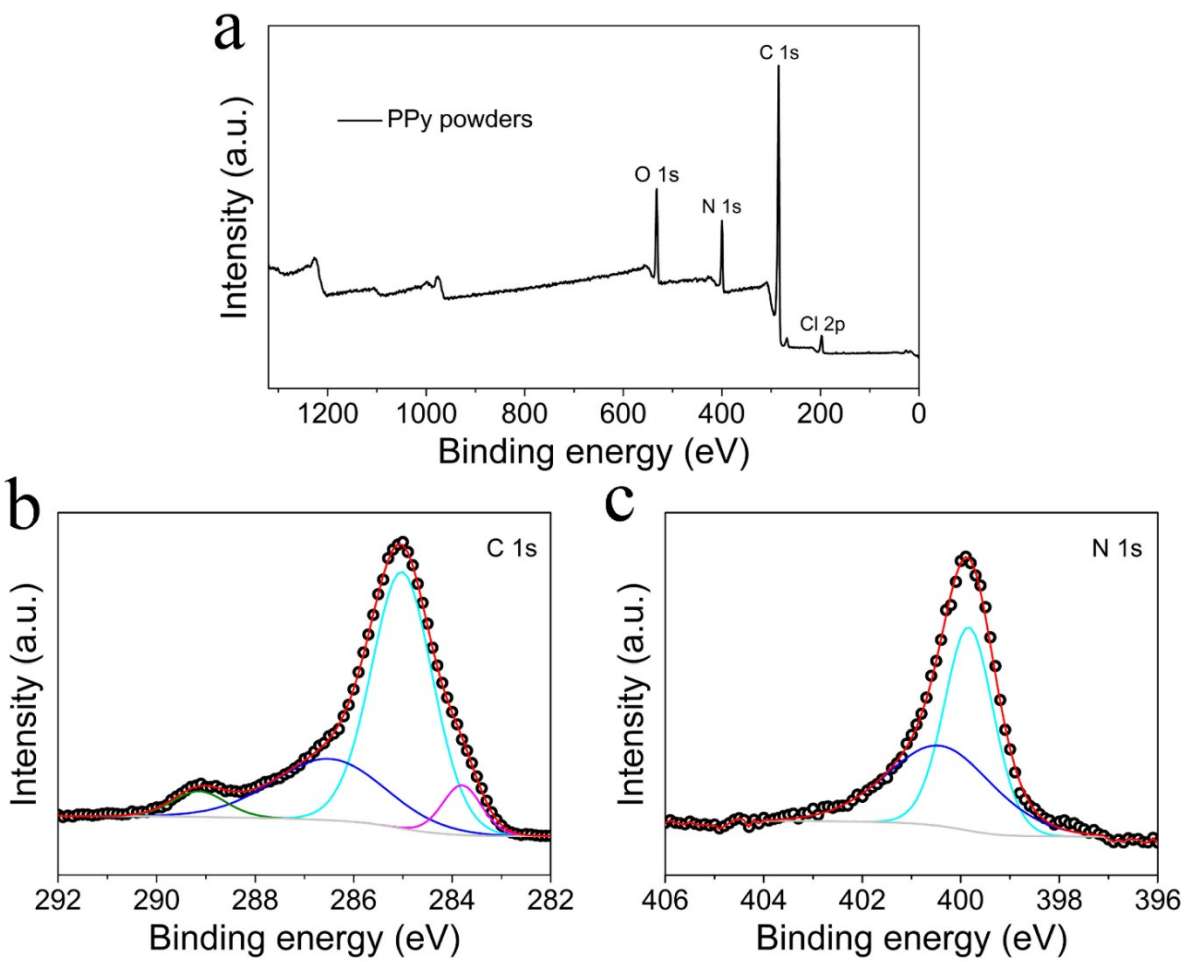


**Figure S3** (a) XPS survey spectrum of the PPy powders; (b) high-resolution C 1s and (c) High-resolution N 1s.

**Table S1** Assignment of XPS peaks

| | After compression | Assignment of peaks | Ref |
|---|---|---|---|
| C1s | 283.8 eV | β-carbon of the pyrrole rings | [1-3] |
| | 285.0 eV | α-carbon of the pyrrole rings | |
| | 286.5 eV | C=N, C-OH and C-$NH^+$ (polaron) bonds | |
| | 289.1 eV | π–π* satellite | |
| N1s | 399.8 eV | Neutral amine nitrogen (-NH-) | [4] |
| | 400.4 eV | -$NH^+$- (polaron) | |

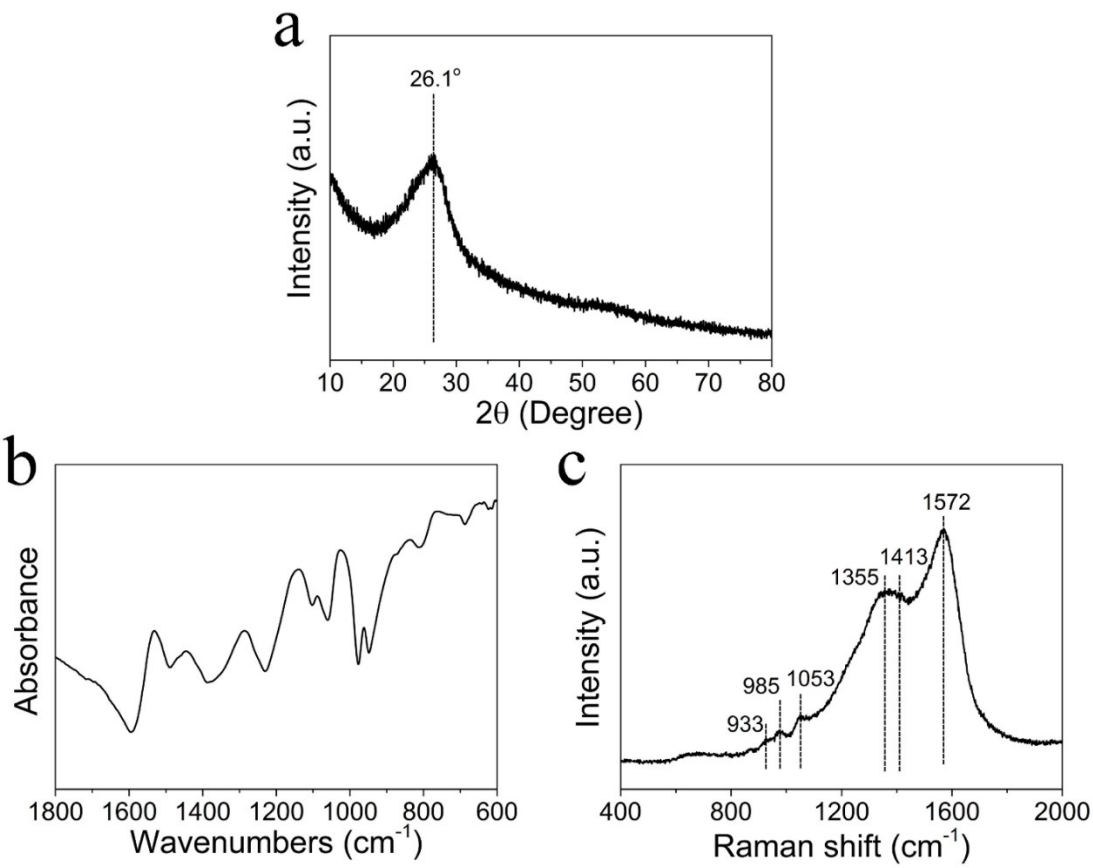


**Figure S4** (a) XRD pattern, (b) FTIR and (c) Raman spectra of the prepared PPy plate.

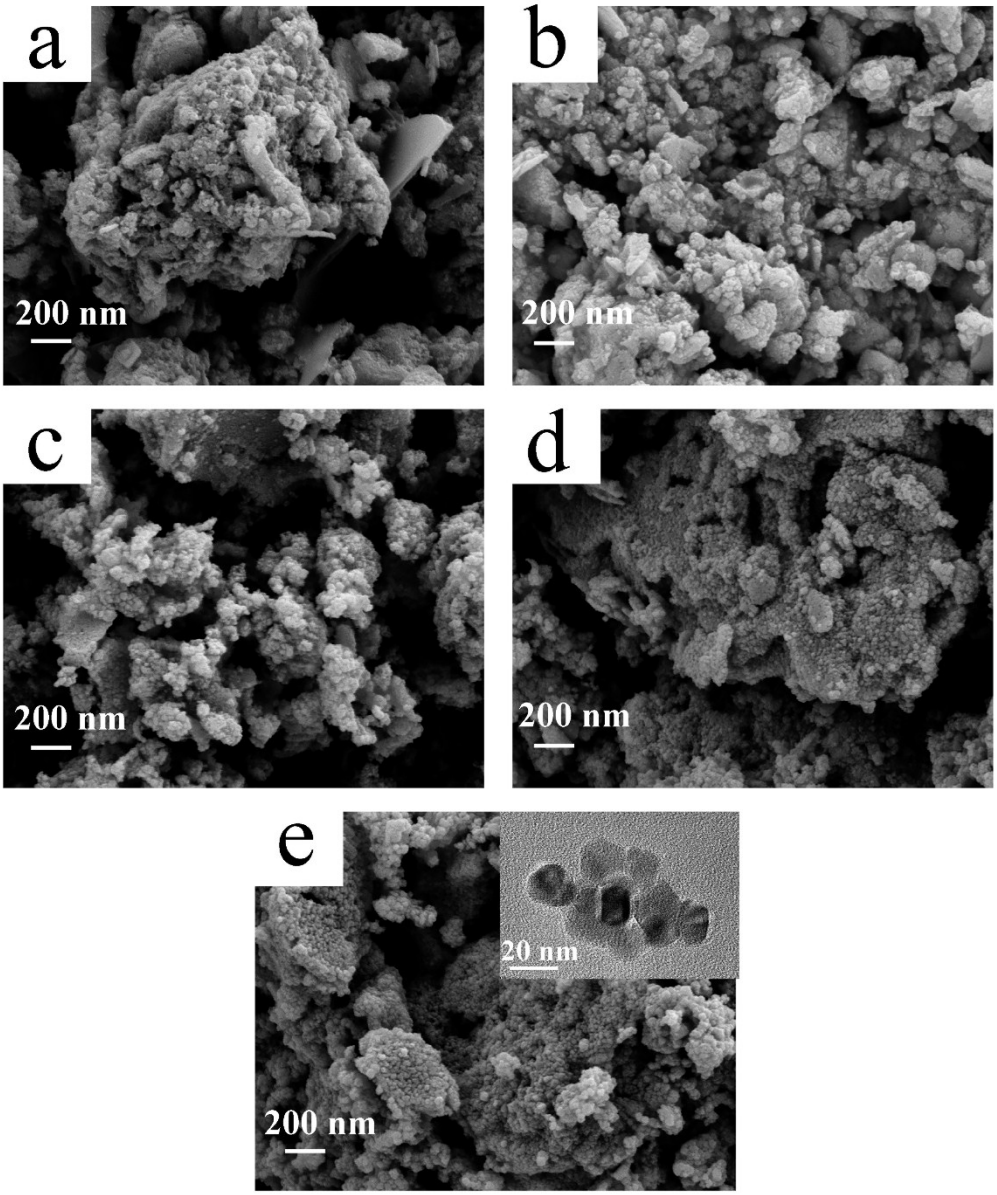


**Figure S5** SEM images of the samples obtained from different calcination temperature of tin oxide precursor: (a) No heating; (b) 200 $^{o}$C; (c) 400 $^{o}$C; (d) 600 $^{o}$C and (e) 800 $^{o}$C. Insert: TEM image of the sample obtained from 800 $^{o}$C.

The spherical powders obtained after calcination at 800 $^{o}$C had an average diameter of 18 nm.

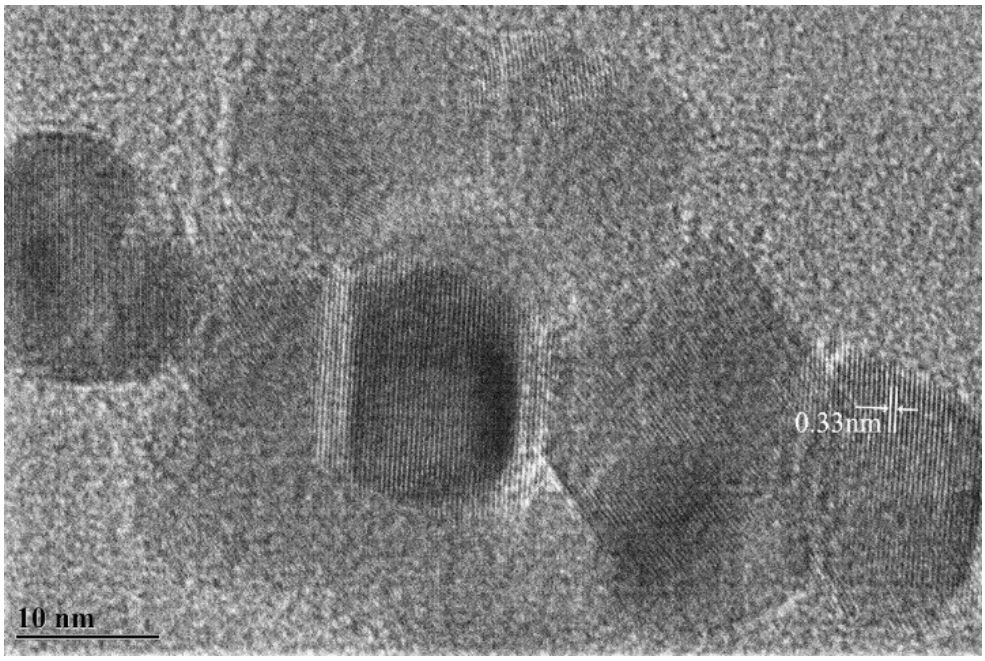


**Figure S6** HRTEM image of $SnO_2$ particles.

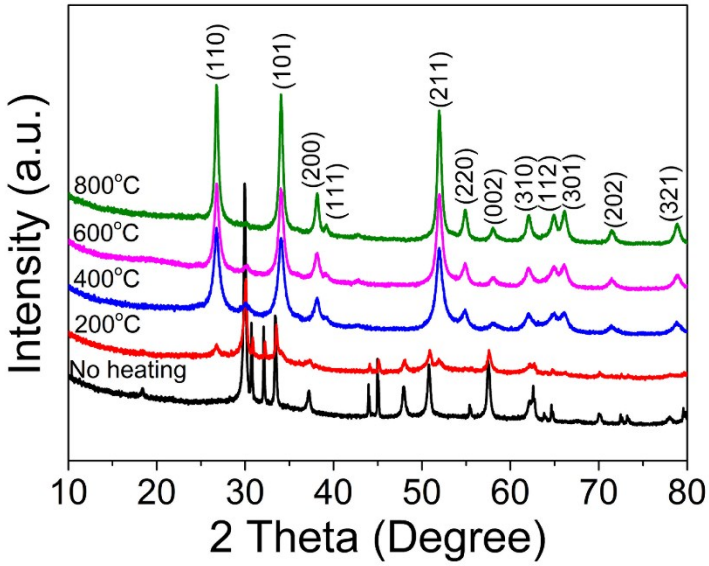


**Figure S7** XRD patterns of as-prepared samples at the different calcination temperature.

The sample calcined at 800 °C shows the rutile phase $SnO_2$ structure with high purity (JCPDS No. 41-1445).

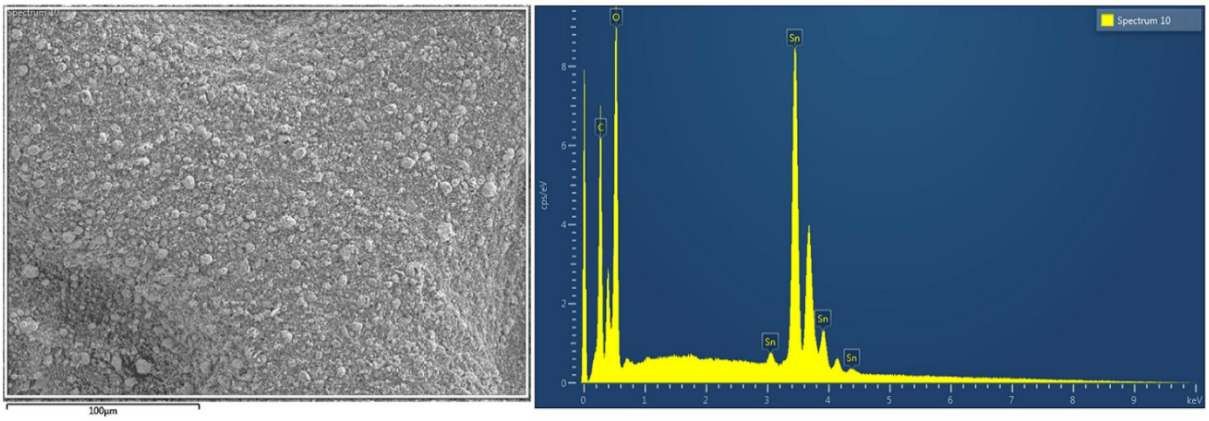


Figure S8 EDX spectrum of as-prepared $SnO_2$ powders calcined at 800 °C.

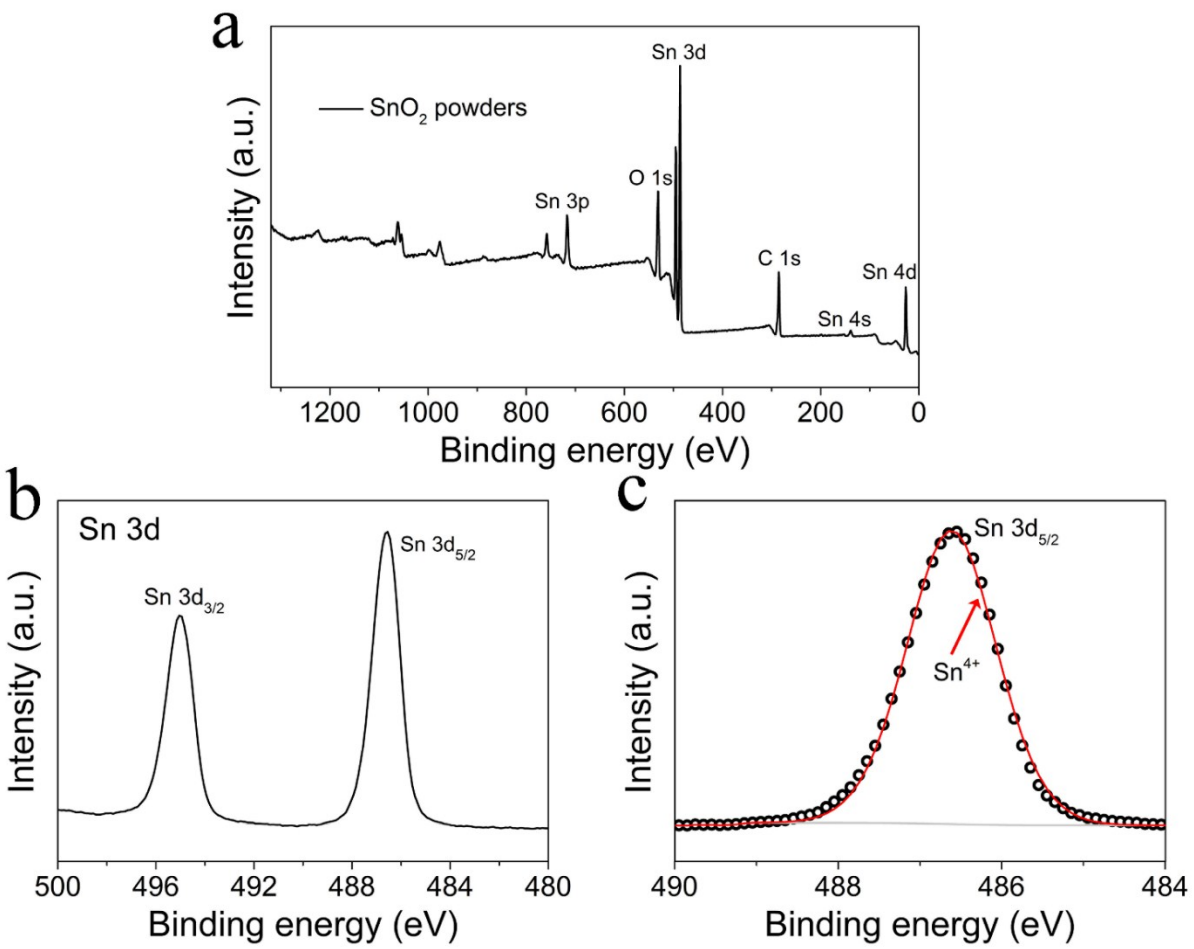


**Figure S9** (a) XPS survey spectrum of the $SnO_2$ powders; high-resolution of (b) Sn 3d and (c) Sn $3d_{5/2}$.

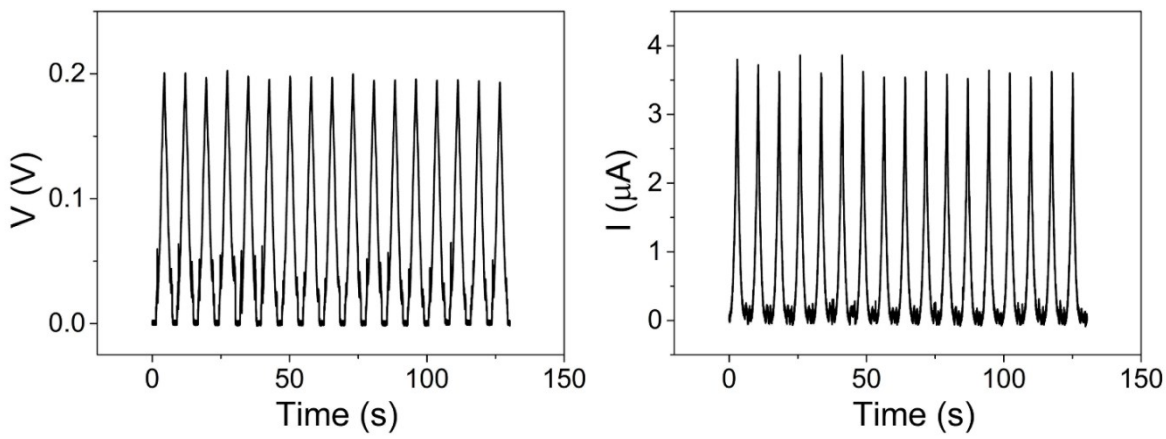


**Figure S10** Voltage and current outputs of the Au/PPy-$SnO_2$/Al system when Al electrode was used as the travelling electrode.

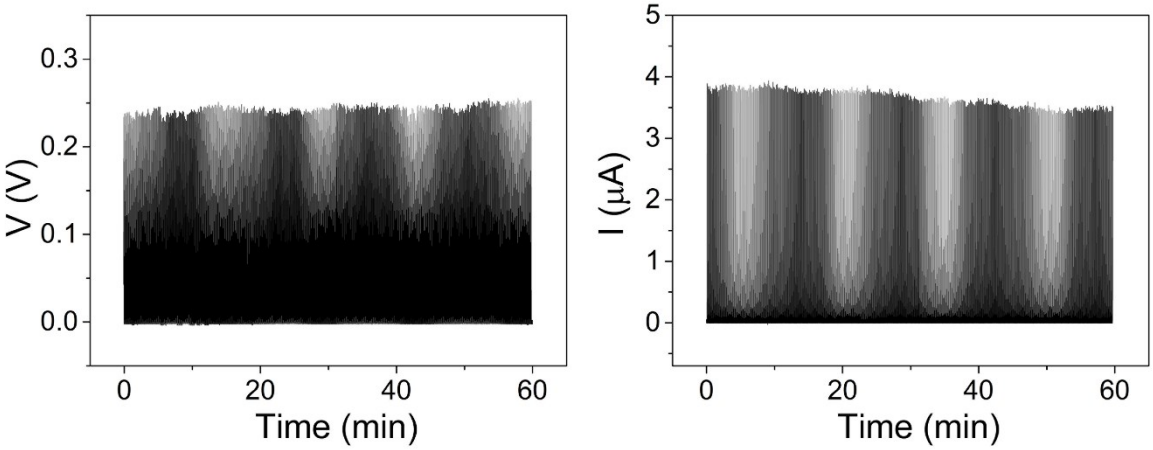


**Figure S11** Open-circuit voltage and short-circuit current outputs of Au/PPy-$SnO_2$/Al device under continuous pressing-releasing impacts for 60 minutes (PPy thickness: 1.064 mm; $SnO_2$ thickness: 0.932 mm; strain level: 3.8%; compression speed: 0.02 mm/s).

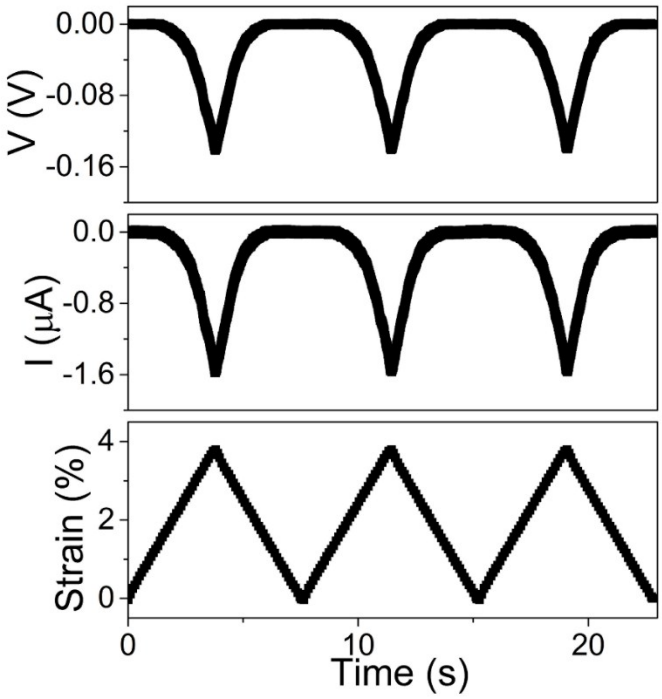


**Figure S12** Electric outputs of the Au/PPy-$SnO_2$/Al device at the reversed electrical connection.

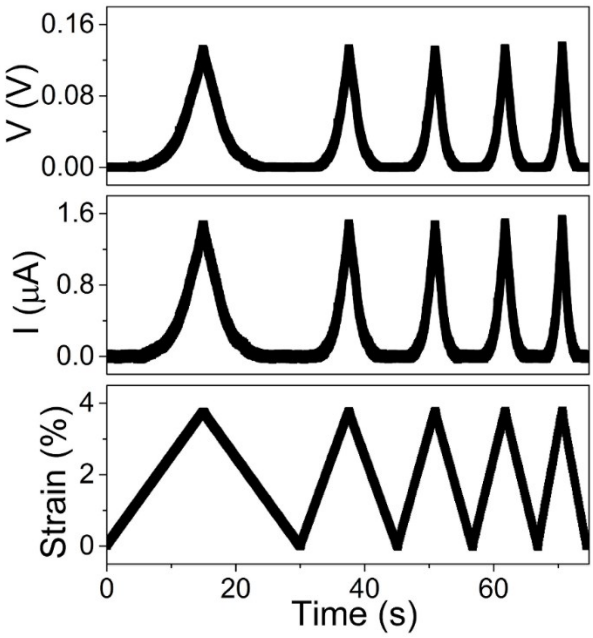


**Figure S13** Electric outputs change with different compression speeds.

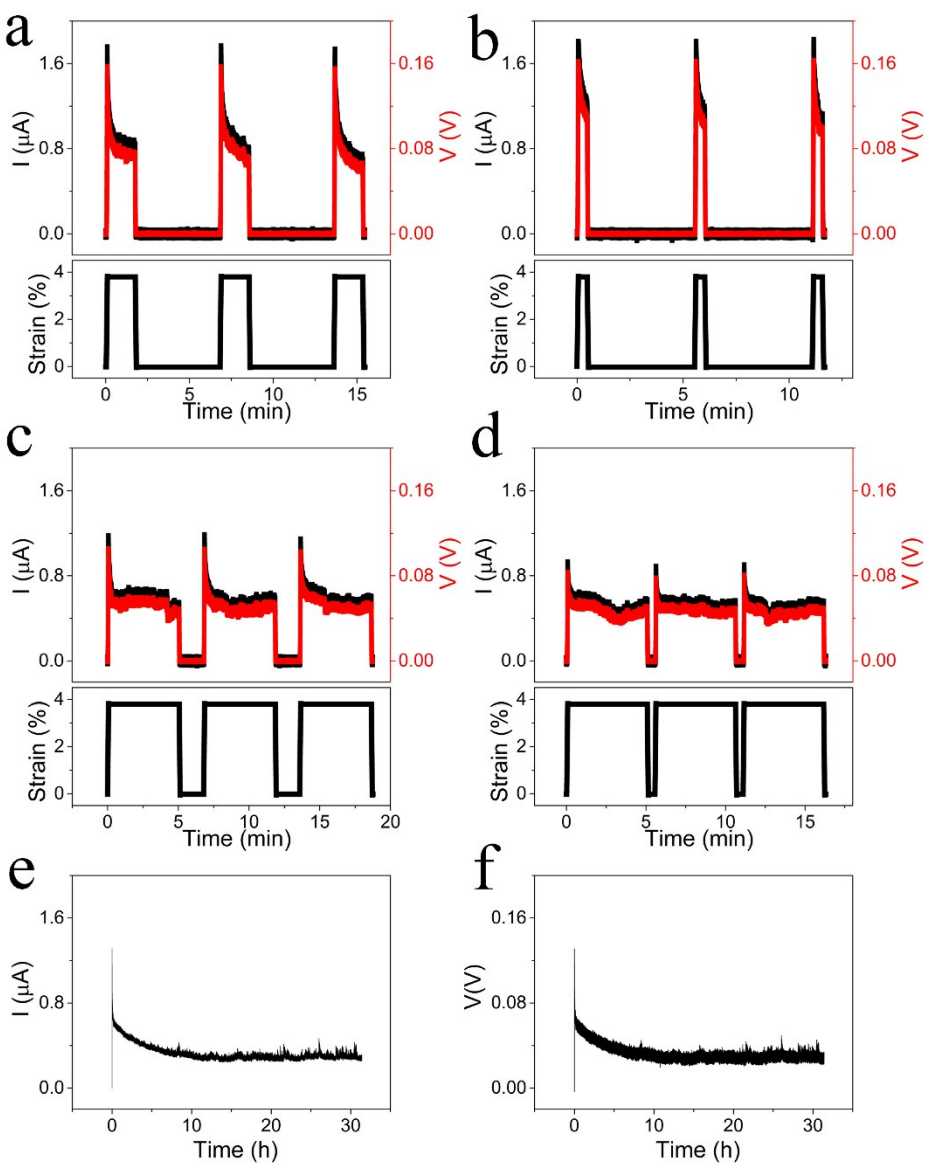


**Figure S14** Effect of compression conditions on electric outputs: (a) $t_1$ = 100 s, $t_2$ = 300 s; (b) $t_1$ = 25 s, $t_2$ = 300 s; (c) $t_1$ = 300 s, $t_2$ = 100 s; (d) $t_1$ = 300 s, $t_2$ = 25 s. Voltage (e) and current (f) outputs of the Au/PPy-$SnO_2$/Al device with a long holding time (~ 32 hours). (PPy plate thickness: 1.06±0.05 mm; $SnO_2$ plate thickness: 0.93±0.05 mm; strain level: 3.8%; Compression speed: 0.02 mm/s; external resistance: 100 kΩ)

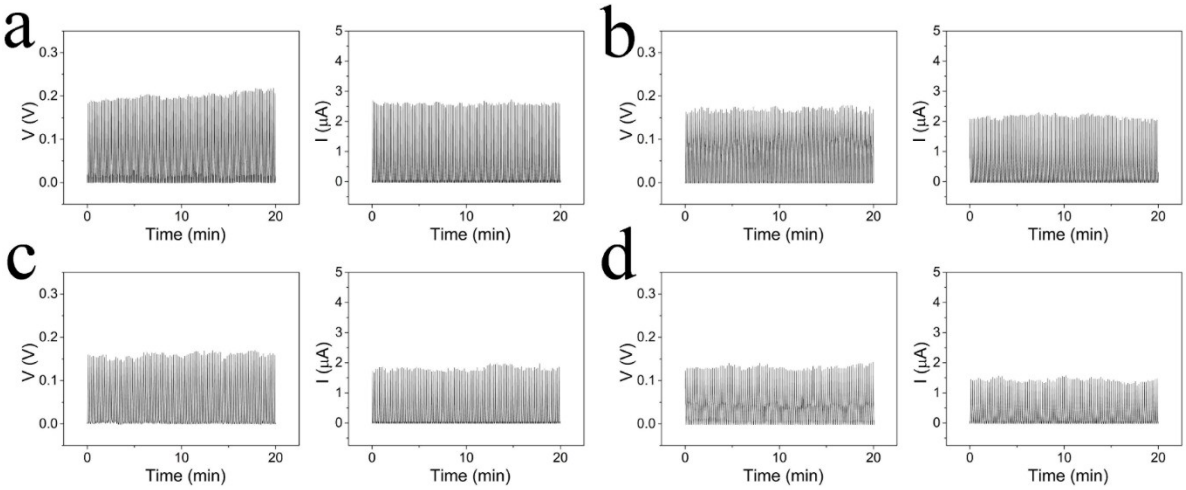


**Figure S15** Electric output signals of Au/PPy-$SnO_2$/Al system with different PPy plate thickness: (a) 1.327 mm; (b) 1.530mm; (c) 1.789 mm and (d) 2.096 mm. ($SnO_2$ plate thickness: 0.932 mm; strain level: 3.8%; compression speed: 0.02 mm/s)

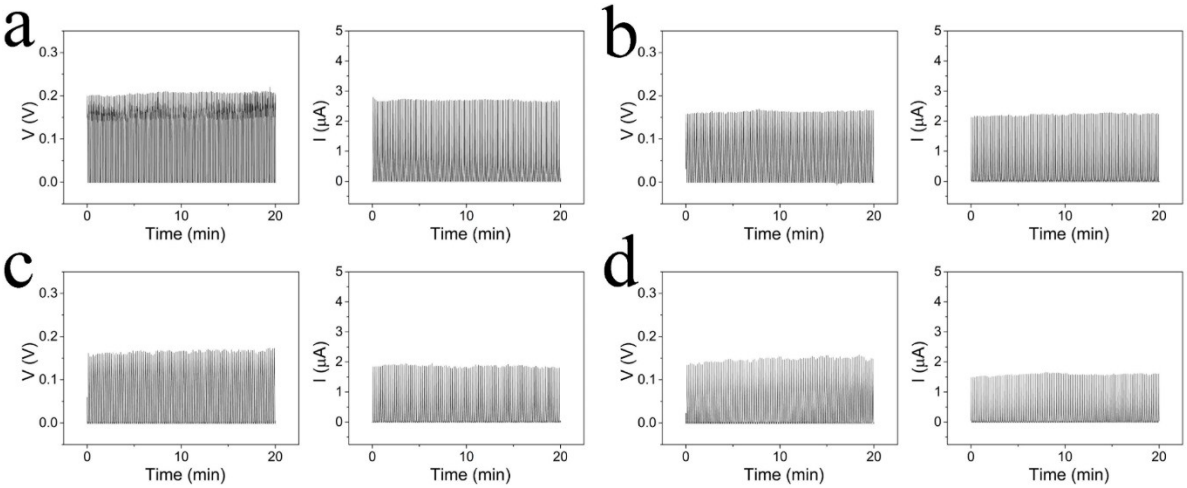


**Figure S16** Electric output signals of Au/PPy-$SnO_2$/Al system with different $SnO_2$ plate thickness: (a) 1.124 mm; (b) 1.3mm; (c) 1.479 mm and (d) 1.809 mm. (PPy plate thickness: 1.064 mm; strain level: 3.8%; compression speed: 0.02 mm/s)

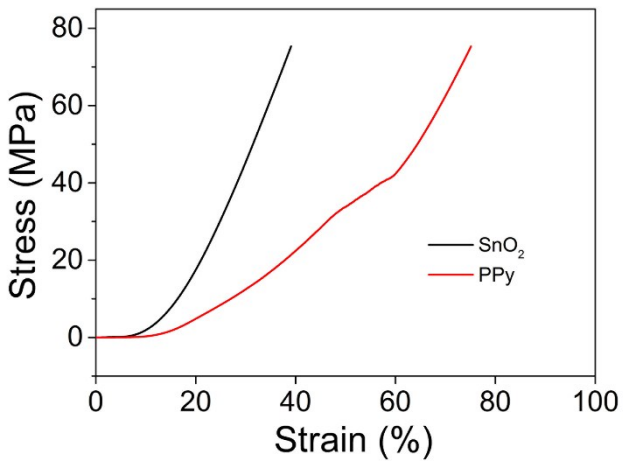


**Figure S17** Stress-strain curves of PPy and $SnO_2$ plate.

The sizes of PPy and $SnO_2$ plate were ϕ13 mm×1.20 mm and ϕ13 mm×0.93 mm. The compression speed was controlled at 0.05 mm/min until the compression force reached 10000 N. According to the stress-strain curves as shown above, the modulus of PPy and $SnO_2$ plates was calculated, about 238.4 MPa and 335.2 MPa, respectively.

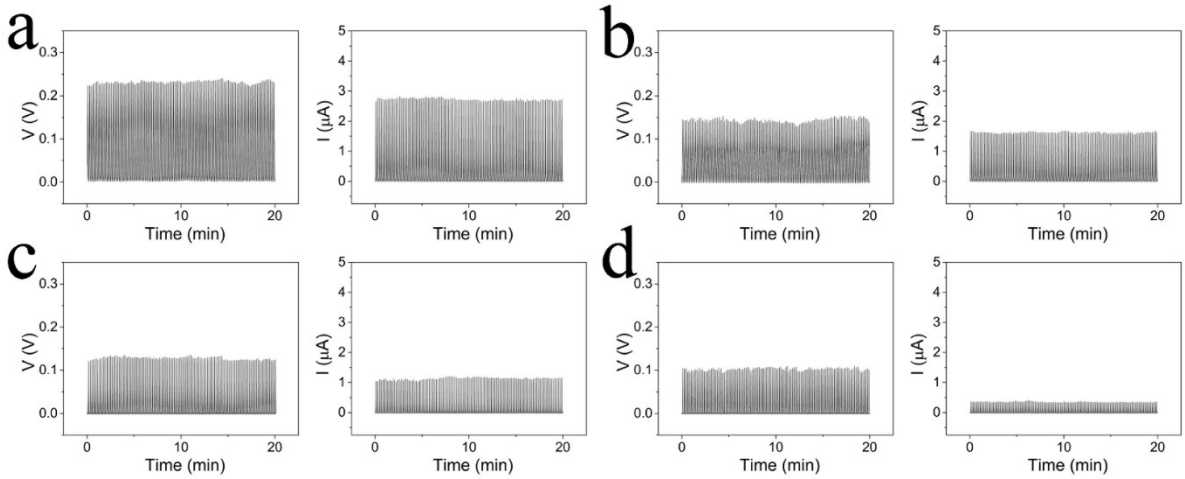


**Figure S18** Electric output signals of Au/PPy-$SnO_2$/Al system with different plate areas: (a) 1.2 $cm^2$; (b) 0.74 $cm^2$; (c) 0.25 $cm^2$ and (d) 0.14 $cm^2$. (PPy plate thickness: 1.064 mm; $SnO_2$ plate thickness: 0.932 mm; strain level: 3.8%; compression speed: 0.02 mm/s)

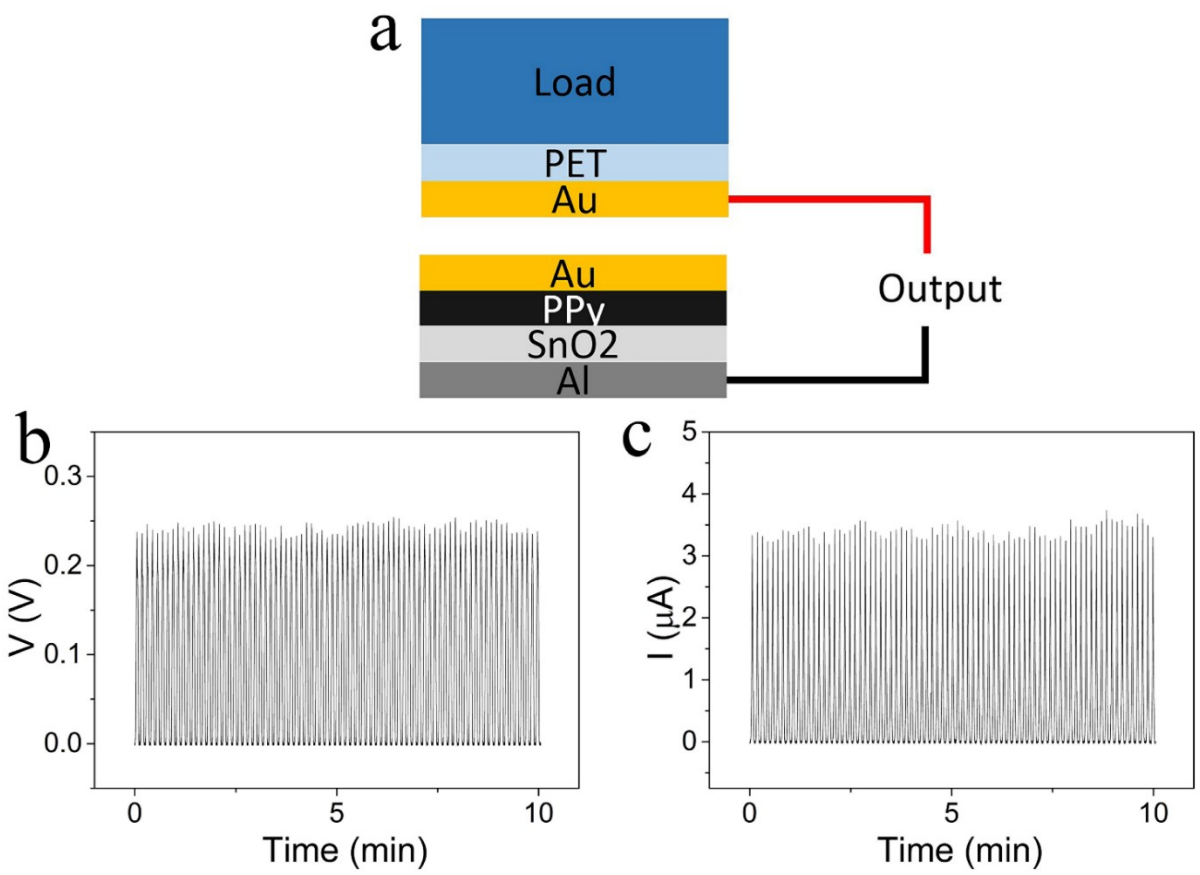


**Figure S19** (a) Schematic of electric output recording; (b) voltage and (c) current outputs of the Au/PPy-$SnO_2$/Al device.

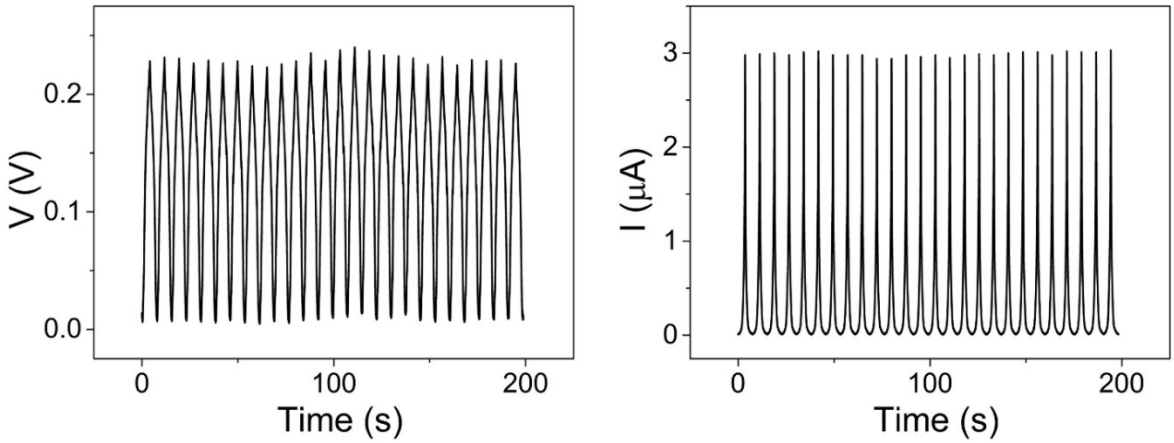


**Figure S20** Voltage and current outputs of the Au/PPy-$SnO_2$/Al system when Au electrodes was closely connected with PPy all the way during compressing-releasing impact (0.2N pre-load).

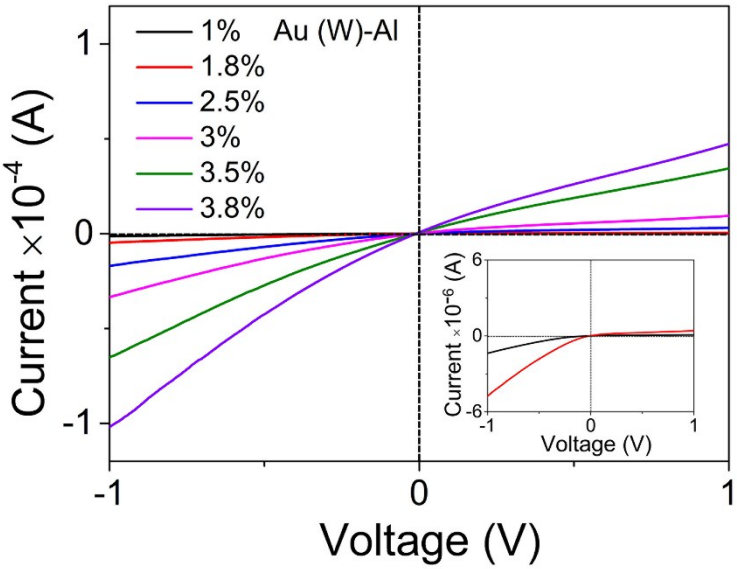


**Figure S21** I-V characteristics of the Au/PPy-$SnO_2$/Al at the different strain levels; insert: the enlarge view of curves at 1% and 1.8% strain level. (Working electrode: Au)

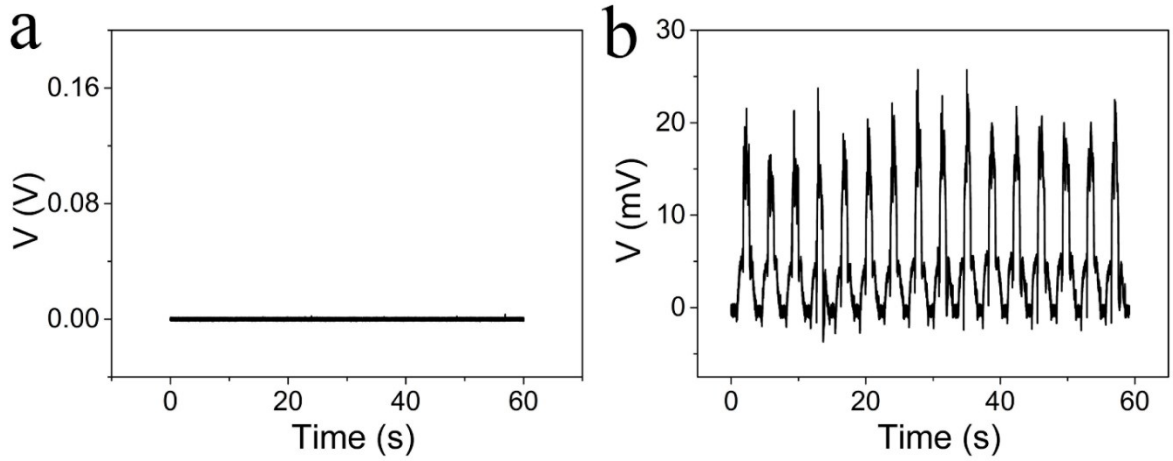


**Figure S22** The electric voltage output of (a) Au/PPy/Au and (b) Al/$SnO_2$/Al devices under compression strain of 3.8%.

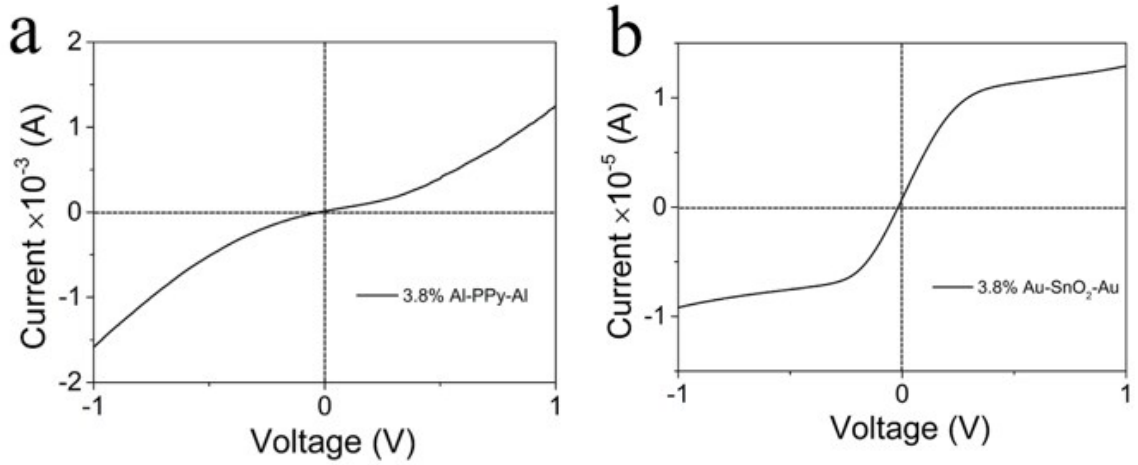


**Figure S23** I-V characteristics of the (a) Al/PPy/Al and (b) Au/$SnO_2$/Au devices at compressed strain of 3.8%.

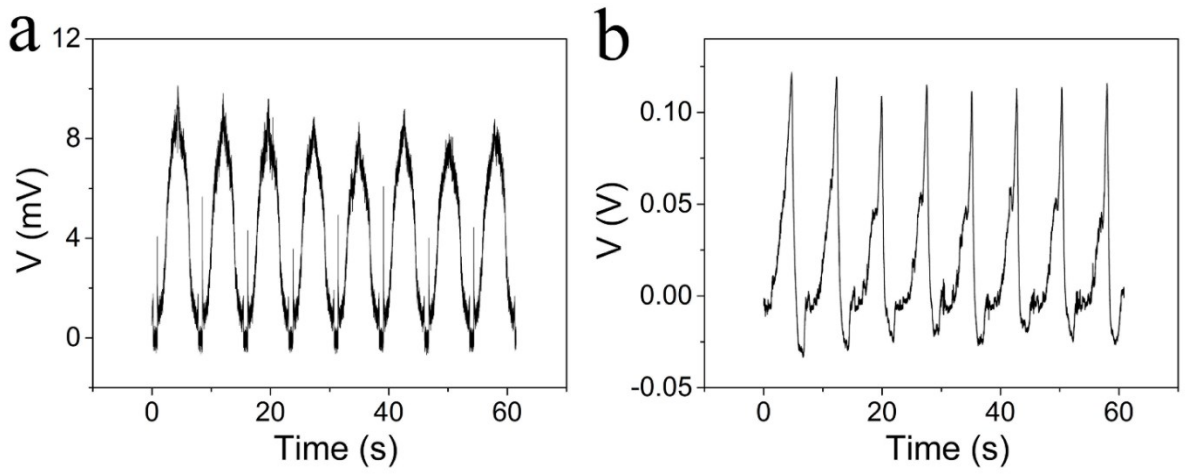


**Figure S24** The electric voltage output of (a) Au/PPy-$SnO_2$/Au and (b) Al/PPy-$SnO_2$/Al devices under compression strain of 3.8%.

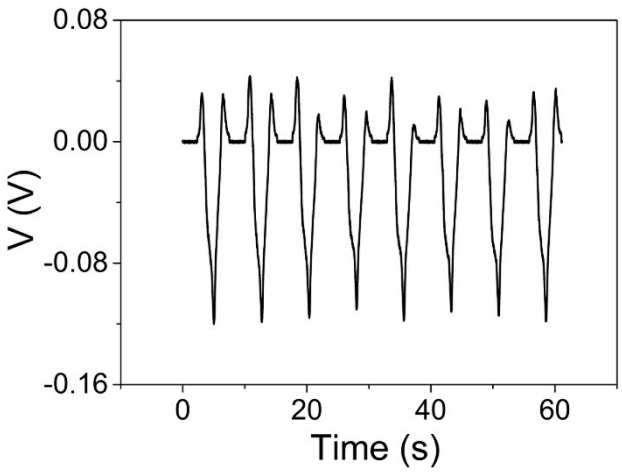


**Figure S25** The electric voltage output of Al/PPy-$SnO_2$/Au device under compression strain of 3.8%.

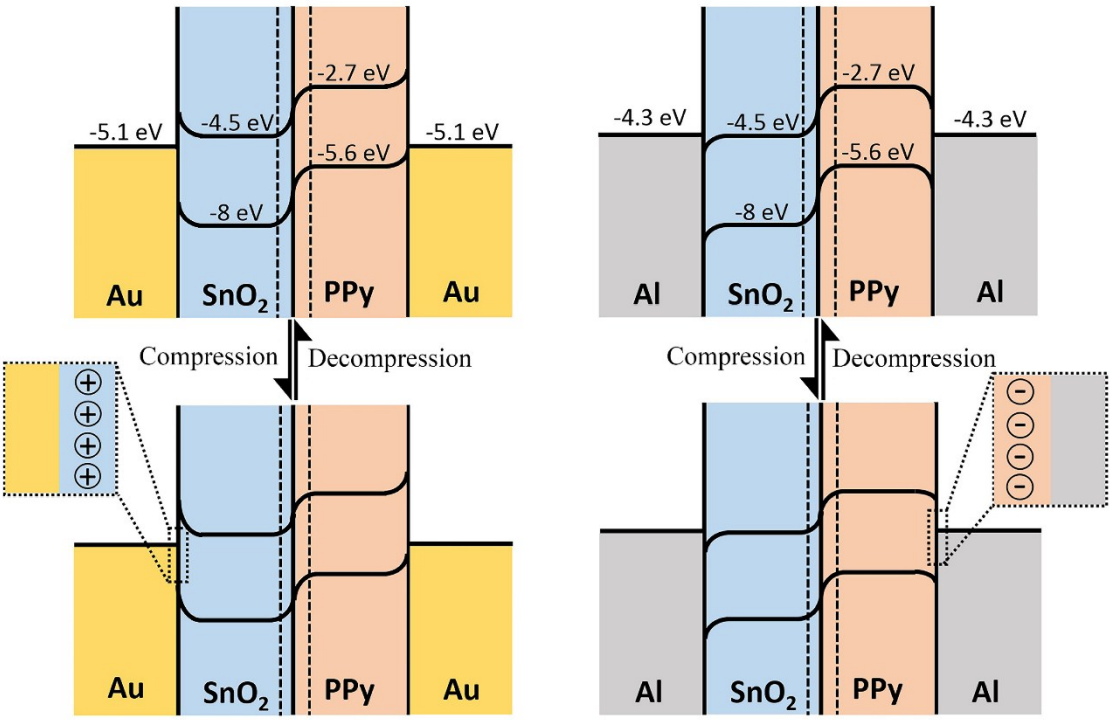


**Figure S26** Proposed energy band equilibria of the Au/PPy-$SnO_2$/Au and Al/PPy-$SnO_2$/Al devices before and after compression test.

Figure S26 show the energy band equilibria of the Au/PPy-$SnO_2$/Au and Al/PPy-$SnO_2$/Al devices before and after compression test. As two non-Ohmic contacts were formed at the both sides of $SnO_2$ layer in Au/PPy-$SnO_2$/Au and also at the both sides of PPy layer in Al/PPy-$SnO_2$/Al devices, respectively, which play the opposite electron transport regulation functions, they resulted in generating AC electric outputs. Some phenomenon happens in the three non-Ohmic contact deice. Therefore, it is believed that single built-in non-Ohmic contact plays the critical role for the DC character of electric outputs generated by polymer-inorganic device.

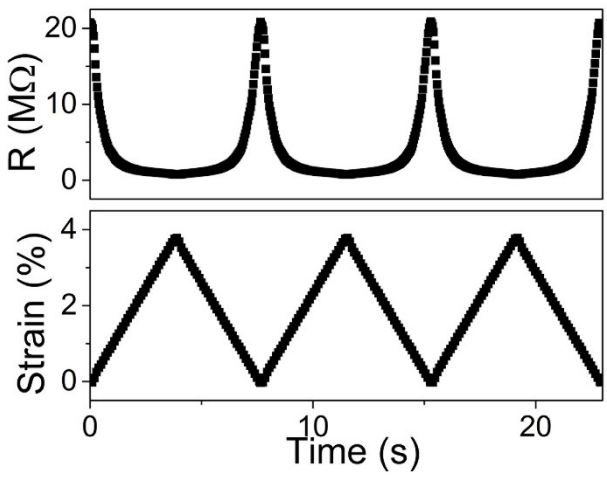


**Figure S27** The electric resistance change under a compressive impact up to 3.8%.

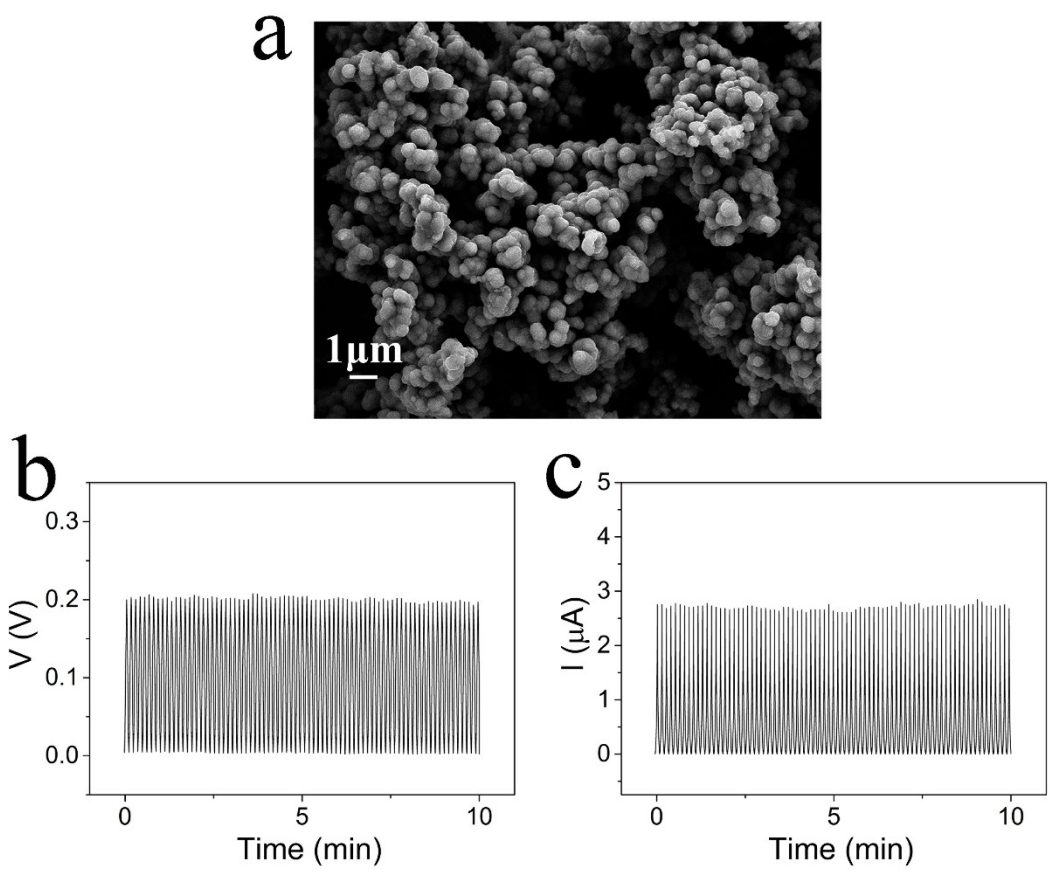


**Figure S28** (a) SEM image of the PPy particles prepared with the $FeCl_3$/pyrrole molar ratio of 4:1; (b) open-circuit voltage and (c) short-circuit current outputs from the Au/PPy-$SnO_2$/Al device under repeated compressive deformation. (Strain level: 3.8%; compression speed: 0.02 mm/s; PPy layer thickness: 1.06±0.05 mm; $SnO_2$ layer thickness: 0.93±0.05 mm)

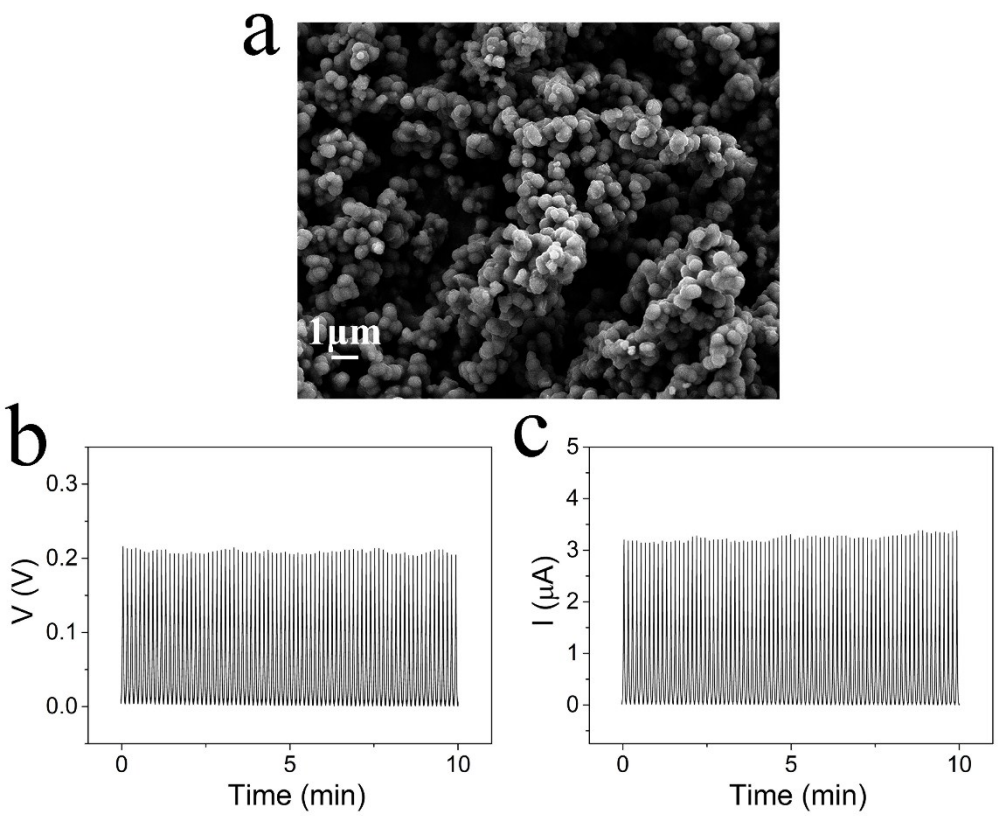


**Figure S29** (a) SEM image of PPy particles prepared with the $FeCl_3$/pyrrole molar ratio of 1:1; (b) open-circuit voltage and (c) short-circuit current outputs from the Au/PPy-$SnO_2$/Al device under repeated compressive deformation. (Strain level: 3.8%; compression speed: 0.02 mm/s; PPy layer thickness: 1.06±0.05 mm; $SnO_2$ layer thickness: 0.93±0.05 mm)

**Table S2** Summary of electric outputs of various devices.

| Device structure | Non-Ohmic contact number | Output feature | I (μA/cm$^2$) | V(V) |
|---|---|---|---|---|
| Au/PPy-$SnO_2$/Al | 1 | DC | 2.71 | 0.25 |
| Au/PPy /Al | 1 | DC | 60.3 | 0.68 |
| Au/$SnO_2$/Al | 1 | DC | 0.38 | 0.08 |
| Al/PPy /Al | 2 | AC | -3.02~1.28 | -0.22~0.05 |
| Au/$SnO_2$/Au | 2 | AC | -0.010~0.008 | -0.004~0.001 |
| Au/PPy-$SnO_2$/Au | 2 | AC | -0.002~0.007 | -0.001~0.009 |
| Al/PPy-$SnO_2$/Al | 2 | AC | -0.17~0.32 | -0.03~0.12 |
| Al/PPy-$SnO_2$/Au | 3 | AC | -0.68~0.15 | -0.12~0.03 |
| Au/PPy-$Al_2O_3$/Al | 1 | DC | 0.004 | 0.006 |
| Au/PPy-ZnO/Al | 1 | DC | 0.013 | 0.019 |
| Au/PANi-$SnO_2$/Al | 1 | DC | 0.47 | 0.14 |
| Au/PEDOT-$SnO_2$/Al | 1 | DC | 1.28 | 0.10 |

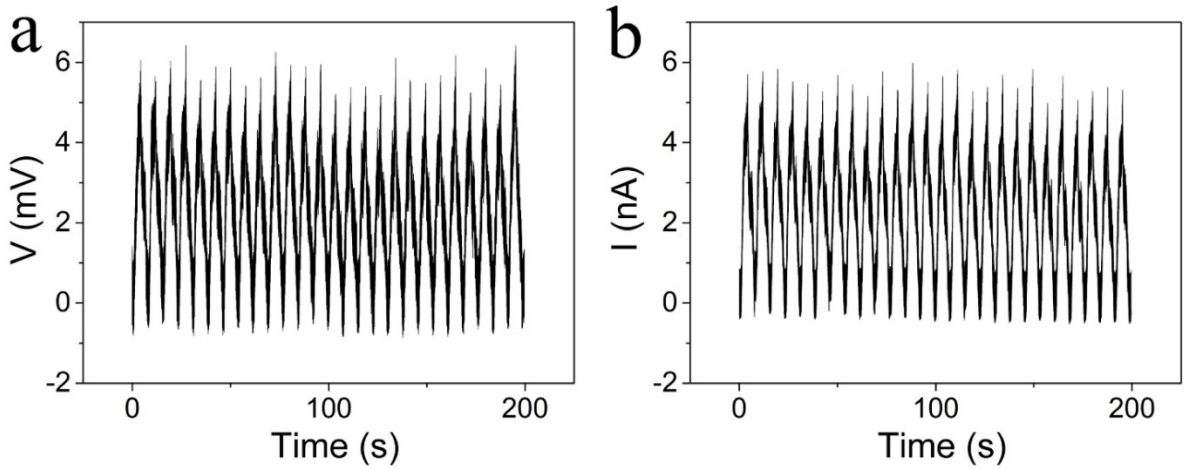


**Figure S30** (a) Voltage and (b) current output of the Au/PPy-$Al_2O_3$/Al device. (PPy plate thickness: 1.064 mm; $Al_2O_3$ plate thickness: 0.936 mm; strain level: 3.8%; compression speed: 0.02 mm/s)

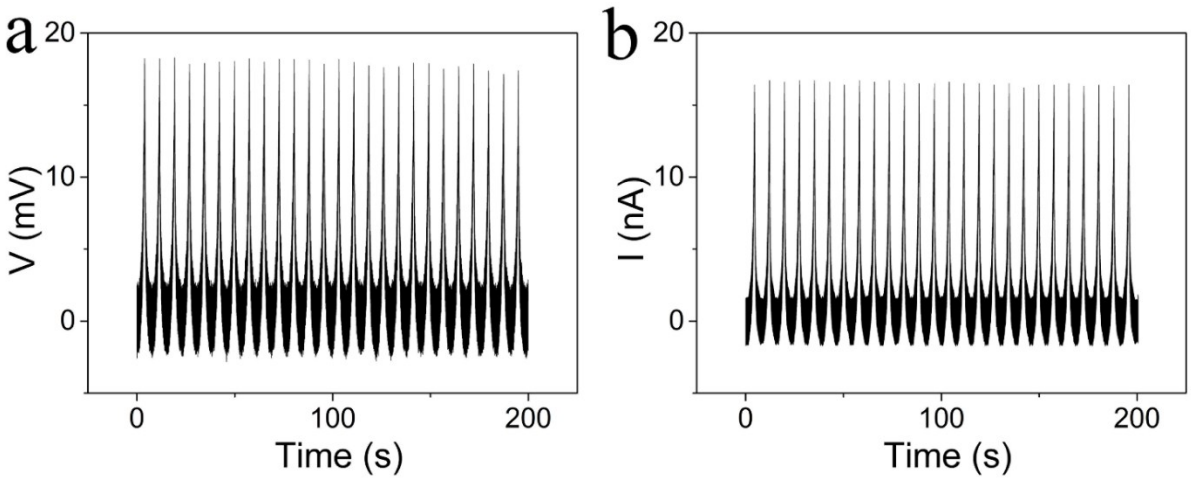


**Figure S31** (a) Voltage and (b) current output of the Au/PPy-ZnO/Al device. (PPy plate thickness: 1.064 mm; ZnO plate thickness: 0.938 mm; strain level: 3.8%; compression speed: 0.02 mm/s)

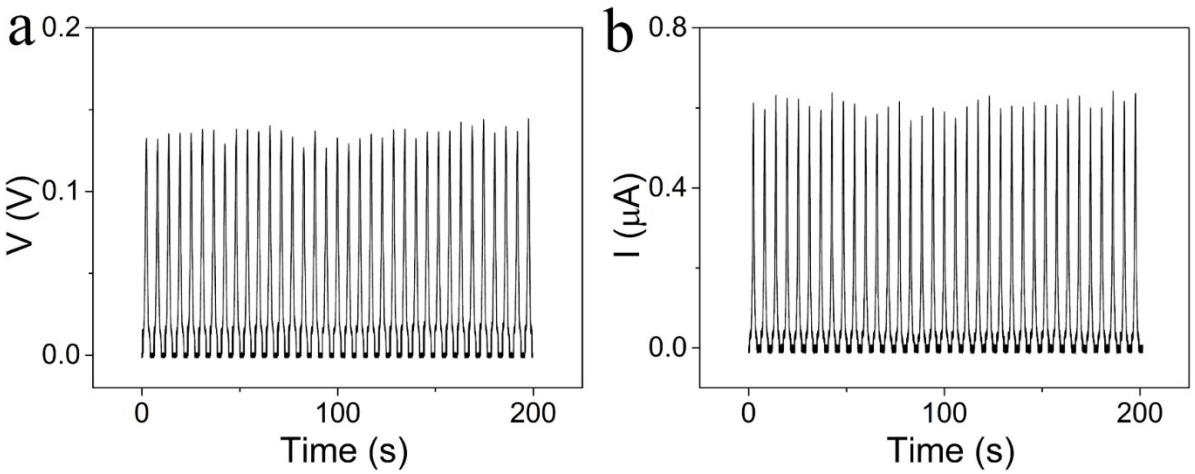


**Figure S32** (a) Voltage and (b) current output of the Au/PANi-$SnO_2$/Al device. (PANi plate thickness: 0.530 mm; $SnO_2$ plate thickness: 0.932 mm; strain level: 3.8%; compression speed: 0.02 mm/s)

PANi preparation method: Polyaniline was synthesized using a vapor phase polymerization method. In brief, $FeCl_3$ fine powder was placed in a glass dish in a vacuum chamber. Aniline was placed underneath the $FeCl_3$ plate. In vacuum, the monomer evaporated to fill the entire chamber in which polymerization tool place on $FeCl_3$ surface. After 48 hour reaction at room temperature, the synthetic powder was added to water and stirred for 48 hours to remove unreacted chemicals and any side products. The powder was then washed with distilled water for several times before drying in a vacuum oven at 60 °C. After drying, the conducting polymer was ground manually into finer powder and then pressed into plates using a steel die (7.5 tonnes for 3 minutes).

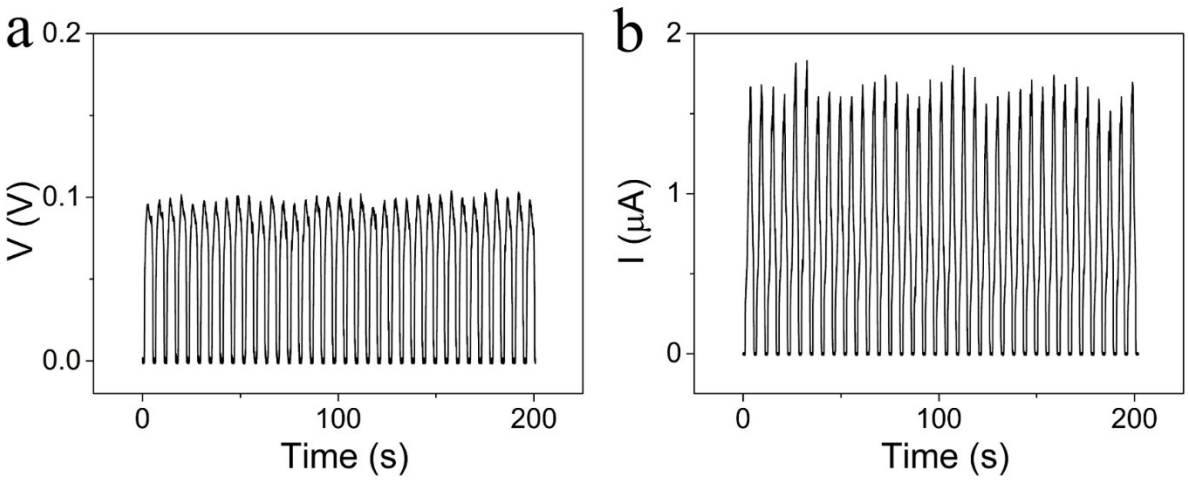


**Figure S33** (a) Voltage and (b) current output of the Au/PEDOT-$SnO_2$/Al device. (PEDOT plate thickness: 0.530 mm; $SnO_2$ plate thickness: 0.932 mm; strain level: 3.8%; compression speed: 0.02 mm/s)

PEDOT was prepared by a similar method to PANi.

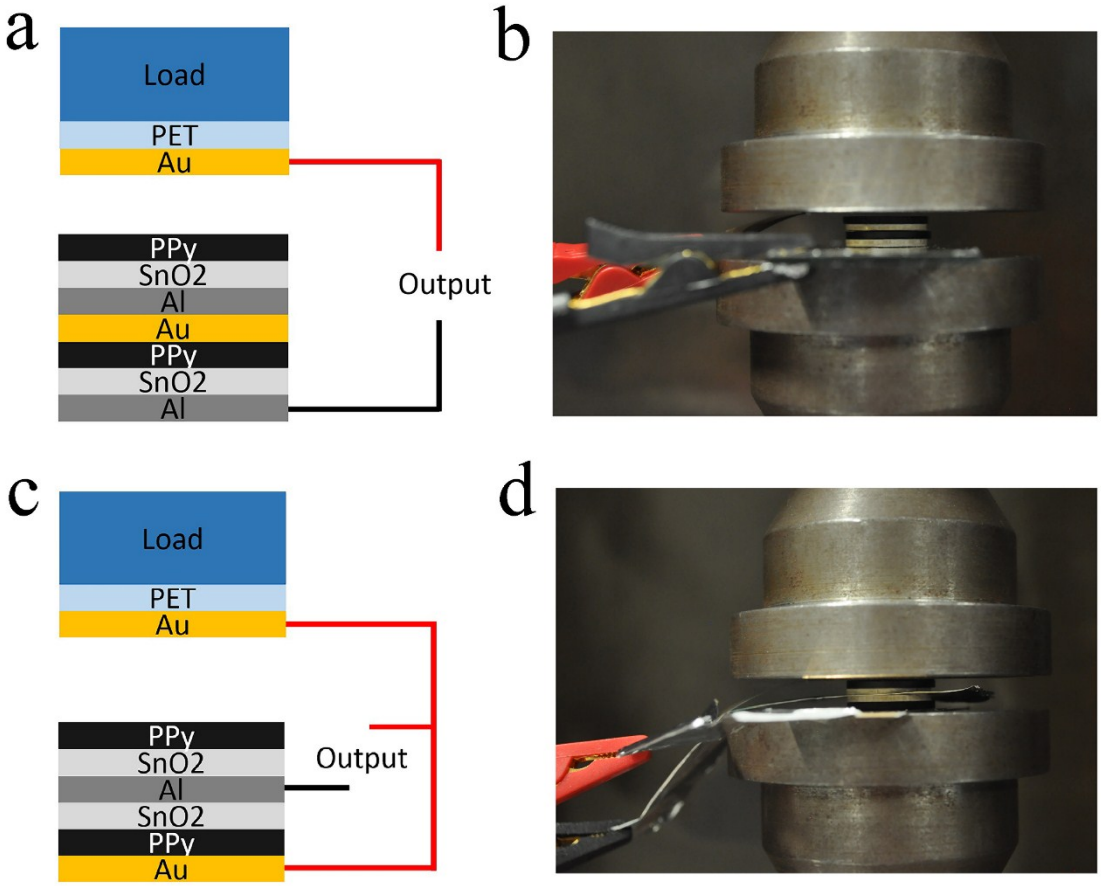


**Figure S34** (a) & (b) Schematic of two devices connected in series and corresponding image, (c) & (d) Schematic of two devices connected in parallel and corresponding image.

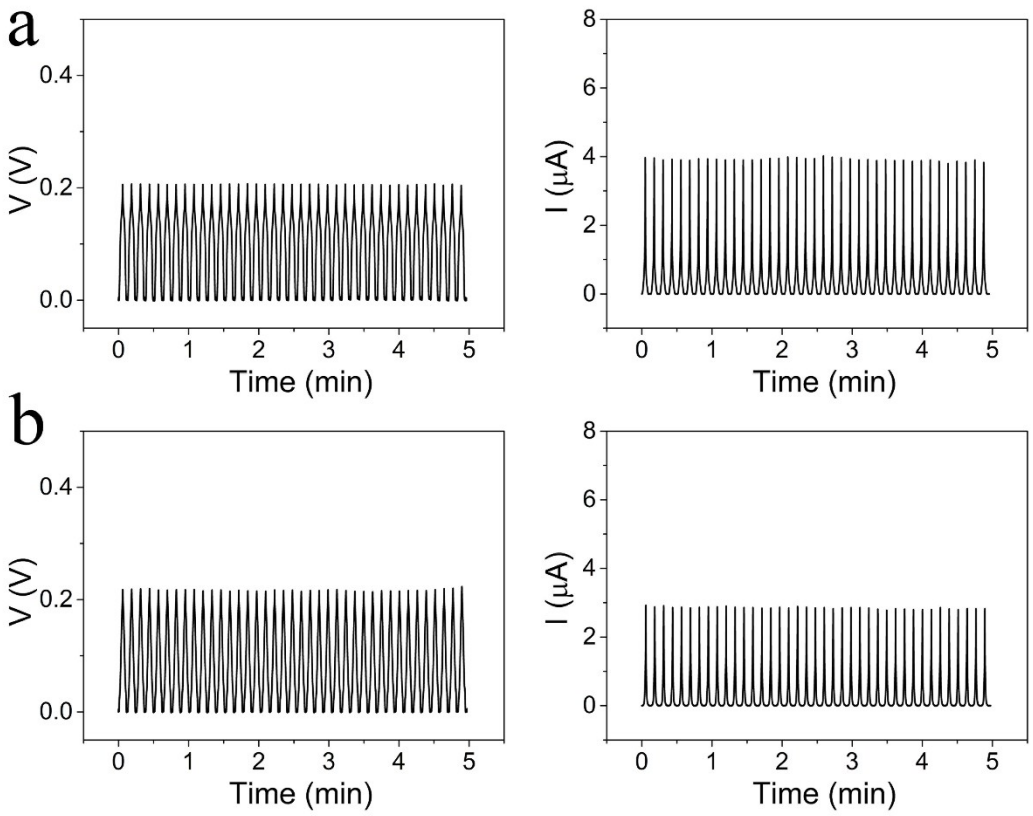


**Figure S35** Voltage and current outputs of (a) device 1 and (b) device 2.

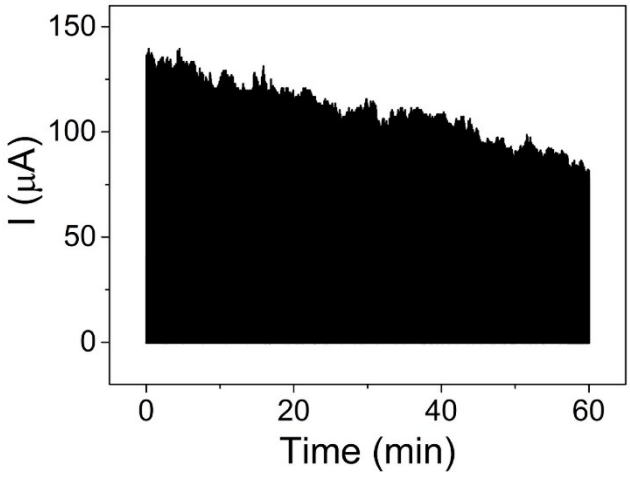


**Figure S36** Short-circuit current outputs of Au/PPy/Al device under continuous pressing-releasing impacts for 60 minutes (PPy thickness: 1.064 mm; strain level: 3.8%; compression speed: 0.02 mm/s).

## References

S1. D. Nam, M. Kim, S. Lim, I. Song and H. Kwon, *J. Mater. Chem. A*, 2013, **1**, 8061-8068.
S2. C. Luk, B. Chen, K. Teng, L. Tang and S. Lau, *J. Mater. Chem. C*, 2014, **2**, 4526-4532.
S3. H. Shao, J. Fang, H. Wang, L. Dai and T. Lin, *Adv. Mater.*, 2016, **28**, 1461-1466.
S4. N. Su, H. Li, S. Yuan, S. Yi and E. Yin, *Express Polym Lett*, 2012, **6**, 697.